Optimal layout of long-gauge sensors for deformation distribution identification

Qingqing Zhang[2], Qi Xia[2], Jian Zhang[*1,2] and Zhishen Wu[2]

[1]*Key Laboratory of Engineering Mechanics of Jiangsu province, Southeast University, Nanjing 210096, China*
[2]*International Institute for Urban Systems Engineering, Southeast University, Nanjing 210096, China*

Abstract. Structural deflection can be identified from measured strains from long gague sensors, but the sensor layout scheme greatly influences on the accuracy of identified resutls. To determine the optimal sensor layout scheme for accurate deflection identification of the tied arch bridge, the method of optimal layout of long-gauge fiber optic sensors is studied, in which the characteristic curve is first developed by using the bending macro-strain curve under multiple target load conditions, then optimal sensor layout scheme with different number of sensors are determined. A tied arch bridge is studied as an example to verify the effectiveness and robustness of the proposed method for static and dynamic deflection identification.

1. Introduction

Deformation as one of the most relevant parameters plays an important role in evaluating bridge safety, and various studies have been carried out to obtain structural deformation indirectly from other measurement (He *et al*. 2012, Yau *et al*. 2013). An improved conjugated beam (ICBM) method has been put forward to estimate distributed deformation of simple structures by using the long-gauge fiber optic sensor, which shows a linear and explicit function between structural deformation and strain distribution (Shen *et al*. 2010). However, the sensor layout scheme greatly influences on the accuracy of the identified deflections from the strain measurements.

At present, the problem of optimal sensor layout (OSP) has received considerable attention over the past few decades, but most of the sensor layout methods mainly focus on the characterizations of modal parameters. Effective influence (EI) method, proposed by Kammer (1990), as one of the most widely OSP-based techniques, has been used for many applications (Worden and Burrows 2001). Based the integration of EI method, the driving point residue (DPR) index was developed, which considered the relative contribution of each mode on candidate locations (Papadopoulos and Garcia 1998). Meanwhile, the kinetic energy (KE) method was proposed by Heo *et al.* (1997) to determine a sensor set that can make the KE of the system maximization. The covariance of target mode shape matrix was utilized for the variance method

---

∗Corresponding author, Professor, E-mail: jian@seu.edu.cn

(Meo and Zumpano 2005), which features the determinant of covariance of the target mode shape matrix as maximized when the optimal sensor configuration is achieved. In structural control engineering, many schemes have been developed for a long time, most of which are based on observation matrix (Abdullah *et al.* 2001) and mathematical standpoint (Buczak *et al.* 2001, Yi *et al.* 2013, 2015, Worden *et al.* 2001). For effective identification of deformation distribution, it is necessary to develop an optimal sensor layout technology for each and every structure. Due to the widely application of tied arch bridge at home and abroad, an optimal layout framework for tied arch bridge is proposed in this article to effectively identify deformation distribution by using the finite long-gauge FBG sensors.

In this article, the authors first investigate the long-gauge fiber optic sensing technology and the theory to identify the deformation distribution of tied arch bridge. It is found that total strain of tie beam from the sensors contains axial strain and bending stain, which cannot be used to estimate deformation distribution directly. Because the deformation distribution of tie beam is mainly dependent on the bending strain, while the axial strain shows no contribution to the deformation. Although improved conjugated beam method (ICBM) can be used to obtain the deformation distribution, it is difficult to effectively identify based on the existing methods of sensor placement. For such a problem, an optimal sensor layout framework designed to identify the deformation distribution is developed based on long-gauge strain. Coupling with mechanical analysis and finite element modeling, a characteristic curve of tied arch bridge is obtained under multiple target load conditions to ensure multiple optimal layout schemes with different sensor numbers. A tied arch bridge is studied to verify the effectiveness of the proposed scheme, and compared with the traditional optimal layout scheme.

2. Theoretical background

2.1 Long-gauge fiber optic sensor

With rapid development of technology, Fiber optic sensor (FOS) is expected to be an achievement in updating sensing techniques. Owing to such potential advantages as electromagnetic noise immunity, geometric versatility, and easy multiplexing capability, FOS is playing an increasingly important part in health monitoring of various structures. However, one of the significant limitations of traditional 'point' sensing is that it may not reflect a local damage unless the sensors can exactly cover the damaged region. Due to the limitations of 'point' sensing, a long-gauge Fiber Bragg Grating (FBG) sensors array has been developed to fit the actual civil engineering (Li *et al.* 2007). Differencing from a majority of FBG sensors that act as localized strain gauge or temperature measurements in the application of monitoring concrete structures (Yung *et al.* 2004, Zheng *et al.* 2010, Lei *et al.* 2013), this sensor presents a "long-gauge" configuration for "distributed layout," which is capable of precisely achieving average strain (or say "macro-strain") over a certain gauge of length that up to several centimeters or meters and covering its measurements throughout the full or some areas of a structure.

As the in-tube fiber equipped inside a long-gauge sensor has same mechanical behavior, the strain transferred from the shift of Bragg center wavelength represents the average strain over the sensor gauge length. In order to obtain effective measurements in case of very small strain response or too much environmental noise, an improved packaging design is suggested to enhance the measuring sensitivity of long-gauge FBG sensors by utilizing two materials with different

modulus to pack the optic fiber and impose deformation within the gauge length, which largely depends on the essential sensing part of the FBG. By connecting long-gauge sensors in series, an FBG sensor array can be realized to measure distributed macro-strain. Compared with accelerometers, they can provide the equivalent of dynamic displacement distribution from the distributed macro-strain measurements with no double integration requirement. Therefore, the long-gauge fiber optic sensor is suitable to monitor structural macro-strain response and identify the deformation distribution of structure for structural health monitoring (Li *et al.* 2007, Zhang *et al.* 2013).

2.2 Deformation distribution identification of tied arch bridge

Tie beam, being one of the main stress components, serves as the object of research**.** The collected strain data can be used to directly calculate the deformation distribution of simple structure such as simple support beam by means of improved conjugated beam method (ICBM). For the conjugate beam theory, the bending moment distribution $M(x)$ on the real beam is considered as load distribution on the conjugate beam, and then its corresponding bending moment distribution is equivalent to real beam's vertical displacement distribution $y(x)$. It can be easily found that the bending moment distribution mainly contributes to the deflection distribution, namely, the bending strain exerts a significant impact on deflection distribution. Due to the coupling strain of tie beam, the bending macro-strain has to be separated from the coupling strain measured by long-gauge fiber optic sensors to identify the deformation distribution. Zhang *et al.* (2015) have concluded that for the tied arch bridge with a relatively small width-span ratio the axial strain along the tie beam presents the characteristic of cubic curve, and for the bigger width-span ratio, quadratic curve is suitable to estimate the axial strain along the tie beam. Through the top and bottom sensors attached on the beam, the bending macro-strain of tie beam can be extracted by subtracting the axial strain from the total strain. The ICBM method is briefly introduced in the following section.

For the Euler-type beam, the relation among its bending macro-strain, curvature and bending moment are linear shown below

$$\kappa(x) = \frac{\varepsilon(x)}{z} = \frac{M(x)}{EI} \tag{1}$$

$$M(x) = EI\frac{\varepsilon(x)}{z} \tag{2}$$

where z is the distance from the beam's surface to the neutral axis. Assuming that the conjugate beam's load distribution is equal to $\bar{q} = \frac{\varepsilon(x)}{z}$, we can conclude that the corresponding bending moment distribution $\bar{M}(x)$ of the conjugate beam is exactly identical to the real beam's vertical displacement distribution $y(x)$.

Due to the fact that a simply supported beam's corresponding conjugate beam is itself, so the elementary long gauge strain of the real beam and the corresponding load distribution on conjugate beam is shown in Fig. 1 as follows:

For the balance, the reaction at the left support of the conjugate beam is

$$\bar{R} = \frac{L_m}{n} \sum_{i=1}^{n} \bar{q}_i \, (n - i + 0.5) \tag{3}$$
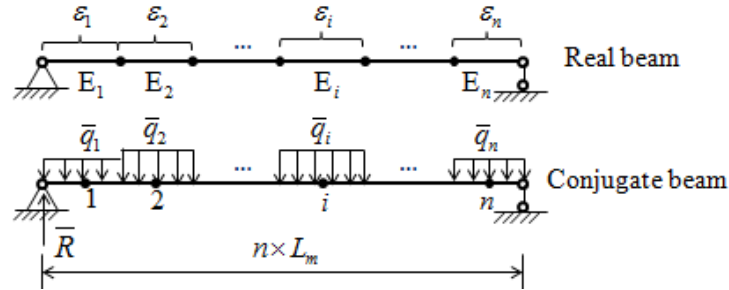
Fig. 1 Scheme of conjugate beam theory for simply supported beam

Where $\bar{q}i = \frac{\varepsilon_i}{z}$, thus the bending moment of midpoint in each element of conjugate beam (i.e., the vertical displacement of the same point in the real beam) is

$$y_i = L_m^2 \sum_{j=1}^{i} \bar{q}_j(i-j) + \bar{q}_i L_m^2/8 \quad (i = 1,2, \dots, n) \tag{4}$$

3. Theory of sensor optimization layout framework

The traditional sensor layout that places the sensors in the most unfavorable loading locations cannot satisfy the accuracy requirement for identifying the deformation distribution by using the long-gauge strain, especially for the tied arch bridge that suffers the complex stress condition. In order to get the effective deformation distribution of structure based on the long-gauge fiber optic sensor, an optimal sensor layout framework is proposed in this article, which provides multiple sensor optimization solutions with different number of sensors.

3.1 Determination the optimization framework

The purpose of optimal sensor layout in this paper is to effectively use the limited sensors for quality estimation of deformation distribution, and for the tied arch bridge, the detaching technology of coupling strain is added into this framework particularly. It is expected that multiple optimal sensor layout schemes can be obtained by this framework to satisfy the requirement for different sensor number. The framework of optimal sensor layout is shown in Fig. 2 and the part of the mechanical modal has been discussed in section 2.2. This part focuses on the finite element analysis and combines with the mechanical modal to analyze the tied arch bridge. Mechanical behaviors of structure under the load conditions can be clearly demonstrated by using the finite element analysis. Since long-gauge fiber optic sensor is applied to monitor the macro-strain response of tied arch bridge, the relation between the gauge length and element length should be considered when building the finite element model. The Fig. 2 shows the proposed framework of optimal sensor layout. Firstly, the target load conditions of tied arch bridge are confirmed. Then under these load conditions the bending macro-strain curves are extracted from the finite element model to form a characteristic curve. The work to detect feature points of characteristic curve is

very important, which mainly affects the optimal sensor schemes .Choosing finite number of feature points to fit a curve, the optimal sensor layout can be finally determined by minimizing the error between the fitting curve and characteristic curve. As shown in Fig. 7, a tied arch bridge is investigated to demonstrate the framework. The tied arch is 64 m in length and 13 m in height with the rise span ration 1/5, and the width of bridge 14 m, the Young's modulus E of tie beam = 34.965 GPa, density ρ=2549. The span is modeled by 64 equal elements connected to 65 nodes regarding the finite element modeling of this tied arch bridge. Gauge length of the long-gauge FBG sensors is one meter. In order to verify the effectiveness of proposed method, the traditional sensor layout that places sensors in the most unfavorable loading locations has been shown in the Fig. 7(b), and results of identified deformation distribution between the traditional method and the proposed method are analyzed in the section 3.

3.2 Multiple target load conditions

To master the most unfavorable load patterns and the general state of vehicle load of tied arch bridge, multiple target load conditions are determined firstly by means of finite element model. The target load conditions are investigated based on two aspects: control sections and uniformly distributed load. Control sections cannot only determine the locations of most adverse load, but also they are used in the load test to ensure a comprehensive and exact scheme of load arrangement for bridge evaluation. The uniformly distributed load is usually applied to simulate vehicle load on the bridge. The load conditions arising from the two aspects may not demonstrate the longitudinal distribution of vehicle but can simulate the worst situation of vehicle load for a real bridge.
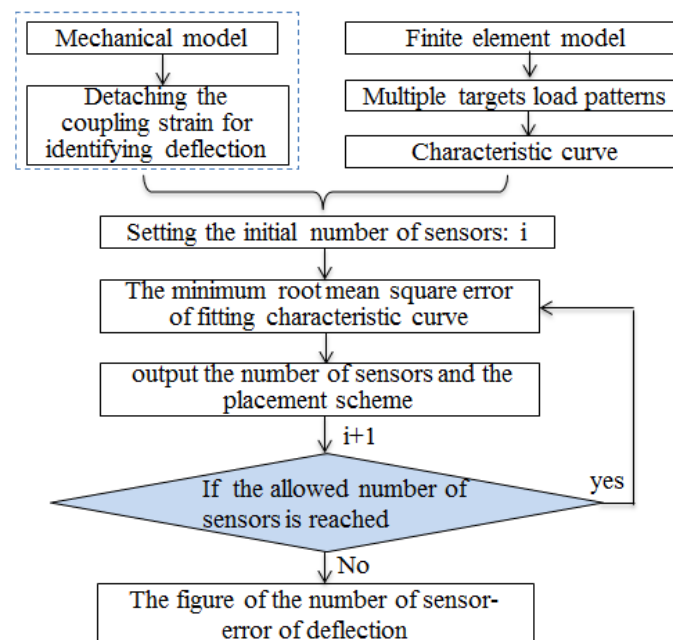

Fig. 2 Framework of optimal layout based on long-gauge fiber optic sensor
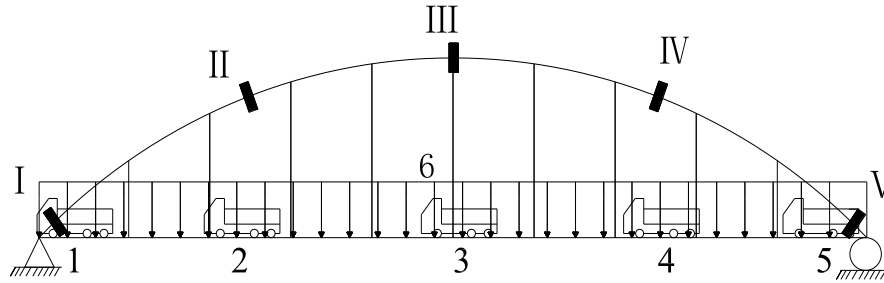
Fig. 3 The target load conditions of the tied arch bridge

The control sections of tied arch bridge are generally comprised of arch vault section, arch foot sections and quarter span sections; likewise, the eighth section can be added to the control sections for long-span bridge. By integrating control sections with uniformly distributed load, the target load conditions of are ensured, including 6 conditions, two of which are arch foot section load conditions, with an arch vault section load condition, L/4 and 3L/4 arch rib section load conditions and uniformly distributed load conditions shown in the Fig. 3. The load conditions will affect the feature points and then affect the precision of calculated displacement distribution. If the load condition is not set in the control section of structure, the extracted feature points will change and finally result in the low accuracy for identified displacement distribution. That's because the key positions may be lost and not selected as the feature points, which have a larger macro-strain and play an important role in all of the feature points.

3.3 Characteristic curve

By using the finite element model, the element bending macro-strain based on long-gauge fiber optic sensor is simulated under target load conditions. The curve shape of bending macro-strain is the main concern, the same load regardless of the load size, are applied to all of the target load conditions. The bending macro-strain curves C1, C2, C3, C4, C5, C6 are extracted under these six load conditions respectively. A point on these curves denotes the macro-strain of an element. Because the magnitudes of these curves are different, all of these curves have to be normalized to stay in the same level, as shown in Eq. (5).

$$GC1 = C1/m1, \ GC2 = C2/m2, \ \cdots\cdots, \ GC6 = C6/m6 \tag{5}$$

Where, m1, m2, ⋯⋯, m6 are the maximum absolute values of every curve. Eq. (5) generates the normalized curves GC1, GC2,⋯⋯, GC6, but these curves fail to demonstrate the characteristic points clearly. Therefore, these normalized curves must be further revised to make the control points, the concave points and convex points obviously. Further normalization processing is as follows.

Calculating the average value a1, a2, ⋯⋯,a6 of each normalized curve, these normalized curves are revised by

$$V1(i) = (GC1(i) - a1)^2, \ V2(i) = (GC2(i) - a2)^2, \cdots\cdots, \ V6(i) = (GC6(i) - a6)^2 \tag{6}$$

Standardized curves V1，V2，⋯⋯,V6 can be obtained using Eq. (6), which magnify the traits of every bending macro-strain curve. Most attention should be paid to the bending macro-strain

curve V6 that is under uniformly distributed load. That's because the curve V6 doesn't present obvious concave and convex point, and easily covers the characteristic of other curves. If the peak value of curve V6 is greater than or equal to the maximum value of other curves, the curve V6 will largely cover these characteristic points. So the curve V6 should be processed to ensure that its maximum value is lower than all of the peak value of other curves, as shown in Fig. 4. It can be seen in the Fig. 4(a) that values of characteristic points generating from curves C1, C2,…, C6 are not of uniform size that only display the characteristics of part of curves, but the curvesV1, V2, …, V6 can highlight the characteristic of all the curves because of the same level of magnitude of characteristic curves.
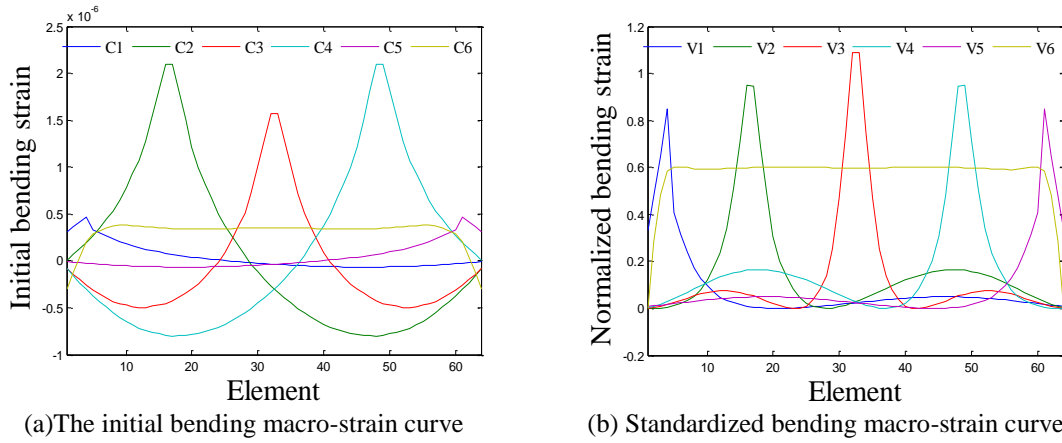

(a)The initial bending macro-strain curve   (b) Standardized bending macro-strain curve

Fig. 4 Bending macro-strain curves under multiple target load conditions

(a)From the original bending macro-strain curves   (b)From the standardized bending macro-strain curves
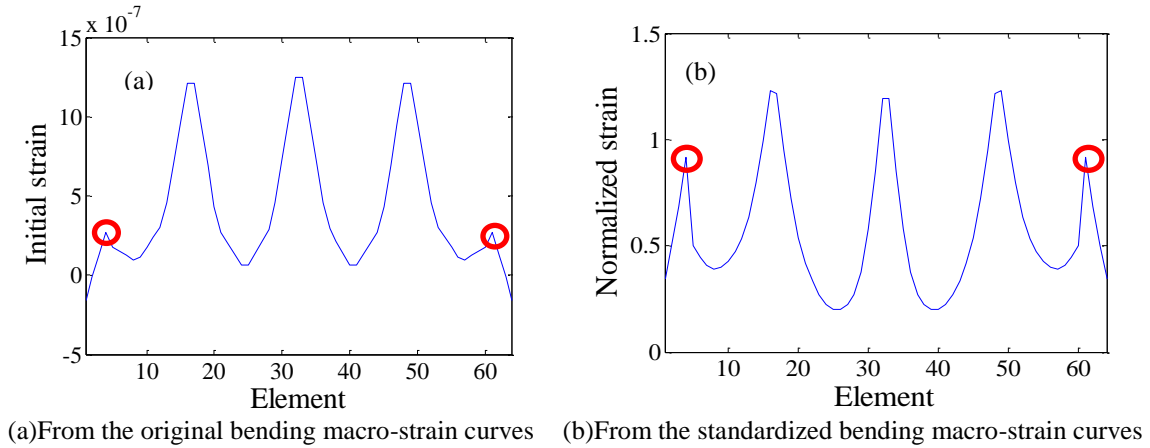
Fig. 5 Characteristic curves

    The curve CB can be obtained by adding all of the standardized curves V1 , V2 , ……,V6, which serves as the characteristic curve of the optimal sensor layout, as shown in Eq. (7).

$$CB(i) = V1(i) + V2(i) + V3(i) + V4(i) + V5(i) + V6(i) \tag{7}$$

Comparing the curve formed by adding all of the original bending macro-strain curves with the characteristic curve, as shown in Fig. 5, the obvious feature points can be easily found in the Fig. 5(a), but there are still feature points that are not obviously, such as the points on the left and right sides of the curve. For all of the feature points, the two feature points are too small to be identified. By using the above method to revise these original curves, the characteristic curve can be got and describes all of the feature points successfully, as shown in Fig. 5(b).

3.4 The optimization scheme

Based on the principle of feature point extraction, the feature points are elected continually with the increasing sensor number until that the number of feature points reaches the upper limit of specified sensor number. The specific steps for extracting the feature points is carried out as follows:

(1) The obvious feature points are firstly extracted from the curve CB. Most of these feature points are turning points, concave and convex points, etc.

(2) To find a feature point from the rest points on curve CB, this point must be staying together with the selected points to fit a curve by interpolation method and enable the fitting curve to have the minimum root mean square error comparing with the theoretical curve, as shown in the Eq. (8).

$$S = \sqrt{\frac{\sum_{i=1}^{N}(X_i - X_i')^2}{N}} \tag{8}$$

Where, N is the total point number on the curve CB, X_i is the value of point i on the fitting curve, X_i' is the value of point i on the theoretical curve .

(3) More feature points are selected from the rest points to form multiple schemes with different number of feature points.

The average transfer error of the fitting curve is essential to demonstrate the accuracy, as shown in the Eq. (9).

$$\bar{d} = \frac{1}{N}\sum_{i=1}^{N}\left|\frac{X_i - X_i'}{X_i'}\right| \tag{9}$$

A series of average transfer errors can be obtained corresponding to different number of characteristic points, namely, the different number of sensors. The tied arch bridge with 64 meters span has been researched and its multiple sensor schemes with different sensor number is shown in Fig. 6. For different sensor number, corresponding optimal sensor scheme supply the minimum average error between the fitting curve and characteristic curve. In Fig. 6, The red line AE denotes the change trend with the change of sensor number. It is not difficult to see that the average error gradually decreases with the increase of the sensor number. There are multiple turning points in the curve AE, such as B,C,D, which divide the curve AE into several curves. Curve AB has heavy gradient and the number of sensors increases from 12 to 18 at this stage, meanwhile the average error decreasing from 16% to 6%. After the point B, the curve AE becomes smooth and gradually tends to be stable.
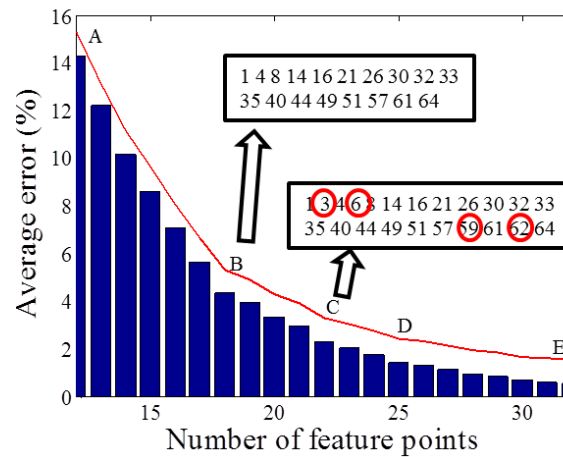
Fig. 6 Average error of fitted curve corresponding to different sensor number

The multiple optimal sensor layout schemes can be confirmed from Fig. 6. Each group of the feature points is an optimal sensor layout scheme corresponding to the specified number of sensor. Considering the budget of practical engineering, the proper sensor scheme is selected for structural health monitoring. However, in order to ensure the accuracy of fitting characteristic curve, the number of sensors should not be less than the number corresponding to the point B.

4. Example of a tied arch bridge

The tied arch bridge with 64 meters length has been described in detail in section 2.3. The proposed optimal layout of this tied arch bridge is analyzed, with result shown in the Fig. 6. According to the figure, a scheme including eighteen long-gauge sensors is chosen for the tied arch bridge. Each long-gauge sensor covering one element is assumed to be installed onto the bottom surface of the tie beam. Owing to the large width-span ratio, three elements1, 32 and 64 have been elected to monitor the axial tensile macro-strain. Therefore, three long-gauge sensors are added to be installed on the top surface of the tie beam as shown in Fig. 7. Moreover, twenty one sensors (18 bottom sensors and 3 top sensors) are selected to be the optimal scheme and the specific sensor layout is shown in Fig. 7(a). The traditional sensor layout, which arranges the sensors in the control sections, is presented to be compared with the optimal layout, as shown in Fig. 7(b). Multiple static load conditions and impact vibration test have been investigated to verify the accuracy of proposed optimal sensor scheme by using the long-gauge fiber optic sensors.

4.1 Static load condition

The six target load conditions are analyzed to verify the optimal sensor scheme, and the result from optimal sensor scheme compares with the result from the traditional sensor scheme.

13m

64 element @ 1.0 m=64m

(a) Optimal sensor scheme

13m

64 element @ 1.0 m=64m

▧ the position of top sensor
— long-gauge FBG sensor
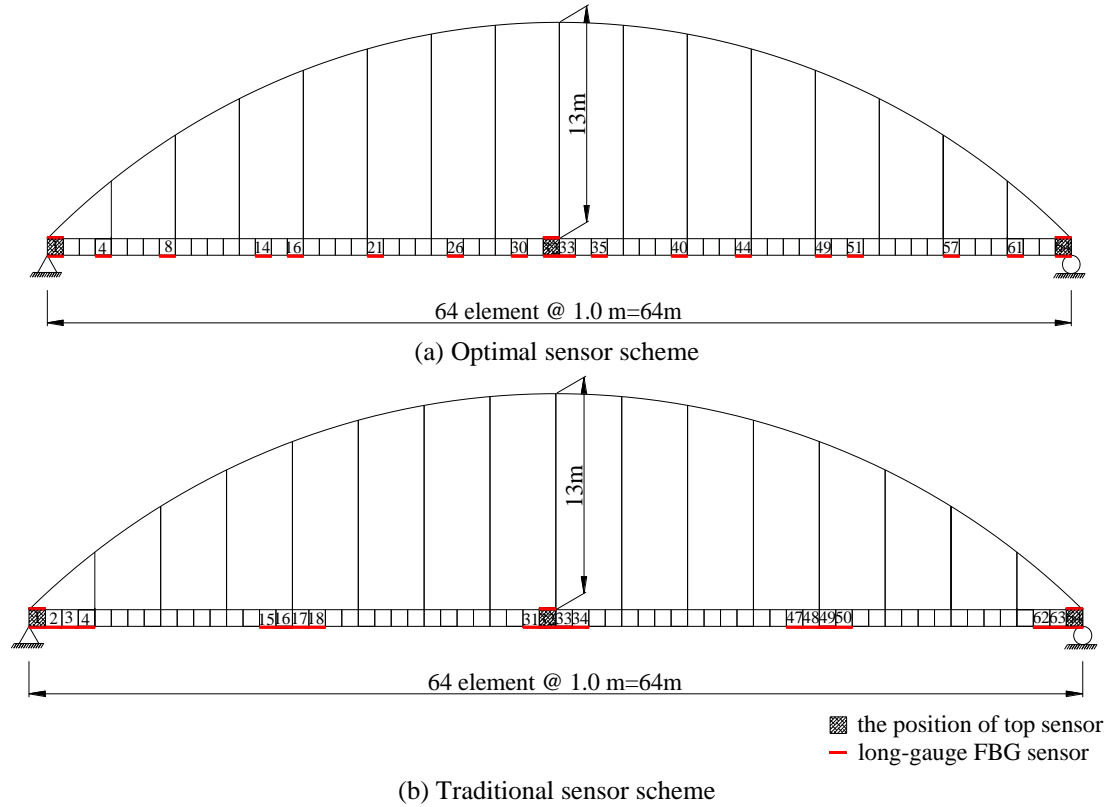
(b) Traditional sensor scheme

Fig. 7 The layout of long-gauge FBG sensor of tied arch bridge

Under these load conditions, the curves of identified deformation distribution (DD) for optimal layout (OP) and traditional layout (TP) are depicted in Fig. 8 to compare with the theoretical curve, with results generating from the load conditions of arch foot section, L/4 arch rib section, arch vault section and distributed load shown in the Fig. 8(a)-8(d) respectively. It is clearly seen that the identified DD curves by OP under four load conditions are basically the same as the theoretical curves, while there is a great deviation between the DD curves identified by the TP and theory curves under the load condition (a) and (c).

To compare the performance of these two sensor layout schemes, all of the maximum values of DD are extracted under the four load conditions, and errors are calculated to be shown in the Fig. 9. The load condition A, B, C, and D in the Fig. 9 correspond to that of (a), (b), (c) and (d) in the Fig. 8 respectively. The result shows that the maximum error from the OP scheme occurs in the load condition C and its value is less than 5%, while maximum error from the TP scheme occurs in the load condition A and its value is close to 50%. It is not difficult to find that the OP scheme is suitable for all the static load conditions.
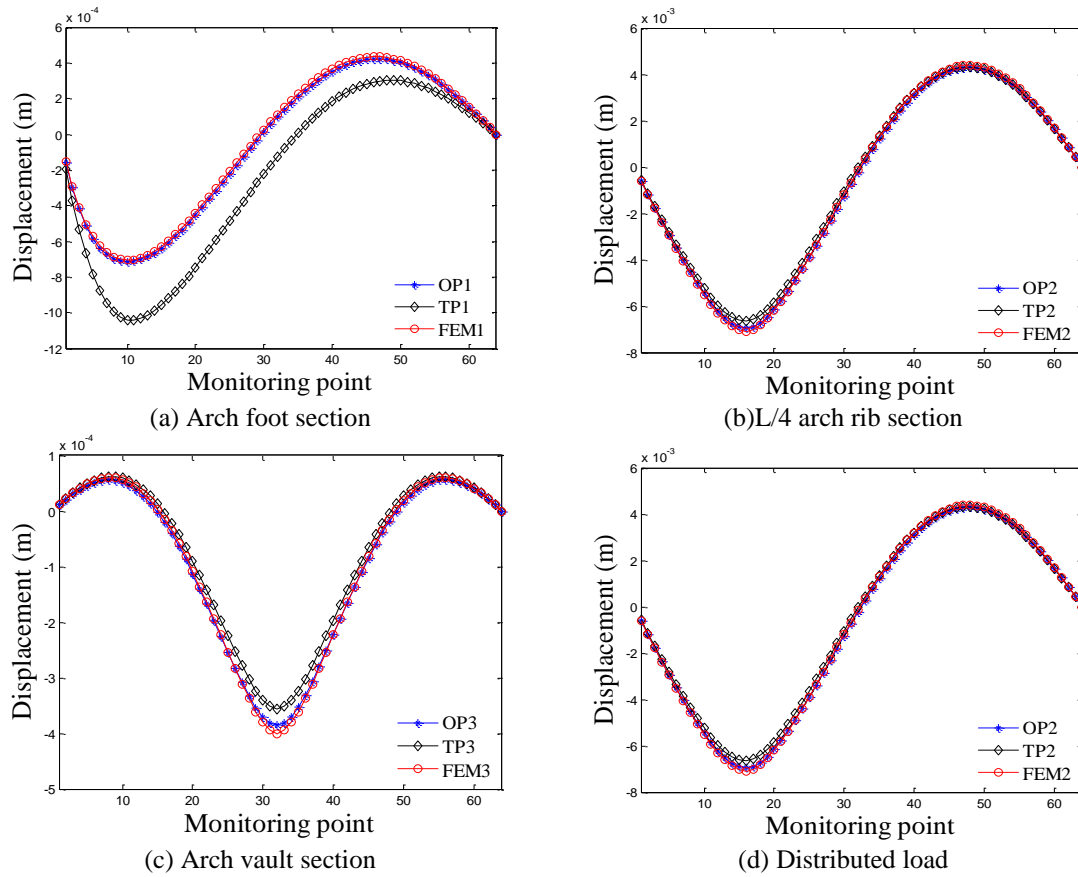
(a) Arch foot section

(b)L/4 arch rib section

(c) Arch vault section

(d) Distributed load

Fig. 8 Identified displacement distribution under four load conditions

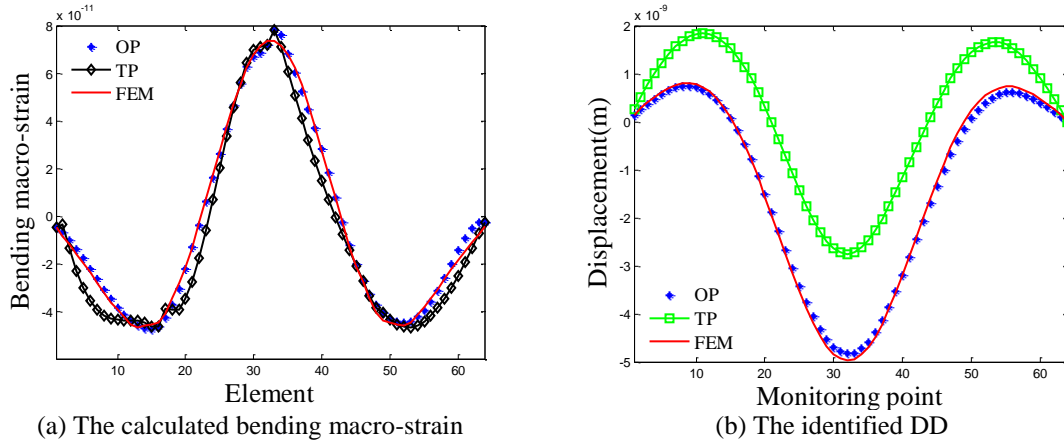Fig. 9 Errors of maximum displacement under four target load conditions

(a) The calculated bending macro-strain   (b) The identified DD

Fig. 10 The bending macro-strain and DD form OP, TP and FEM

4.2 The dynamic load condition

The impact vibration test is designed to identify the DD using OP and TP schemes respectively. It is known from the Fig. 10 that the maximum error of identified DD occurs in the load condition of arch vault section, therefore an impact force is applied in the middle of the span in this part. The time history of long-gauge strain response is simulated by the Sap 2000 software, with 10 percent of white noise added into the dynamic macro-strain data. By analyzing and computing the macro-strain response, the curves of fitted bending macro-strain and identified DD are demonstrated at a random point in time. The Fig. 10 shows the bending macro-strain distribution curves and the DD curves from OP, TP and FEM respectively. It is shown in the Fig. 10(a) that the bending macro-strain curve from OP is basically the same as the theoretical curve, while the curve form TP is similar to the theoretical curve, but doesn't perfectly with the theoretical curve. The identified DD curves from bending macro-strain shown in Fig. 10(b) clearly demonstrate the effectiveness of proposed optimal sensor scheme. But the identified DD from the TP in the maximum displacement still have a large error. It can be seen from result that the small error of bending macro-strain can produce large error in the process of identifying DD.

The time history data of elements that not be installed with sensors are fitted to display macro-strain distribution response of the whole tie beam. In order to assess the performance of the fitting method, element 23 is to be an example to display the results of fitted bending macro-strain and the identified DD from the OP and TP respectively. Fig. 11(a) shows the time histories of bending macro-strain form OP, TP, and FEM, with DD shown in Fig. 11(b). The time history of bending macro-strain obtained from OP is consistent with FEM, while the time history from TP is only perfectly agrees with the FEM when the macro-strain is in the flat section. Although the time history of displacement identified by TP is similar to the FEM, the minimum error of TP is close to 50% in the large deformation positions, so the TP fails to identify the displacement effectively. It is not difficult to find that the proposed optimal sensor layout scheme can effectively identify the displacement time histories of elements that not be installed with sensors, and it is also verified that the identified results is little affected by noise.
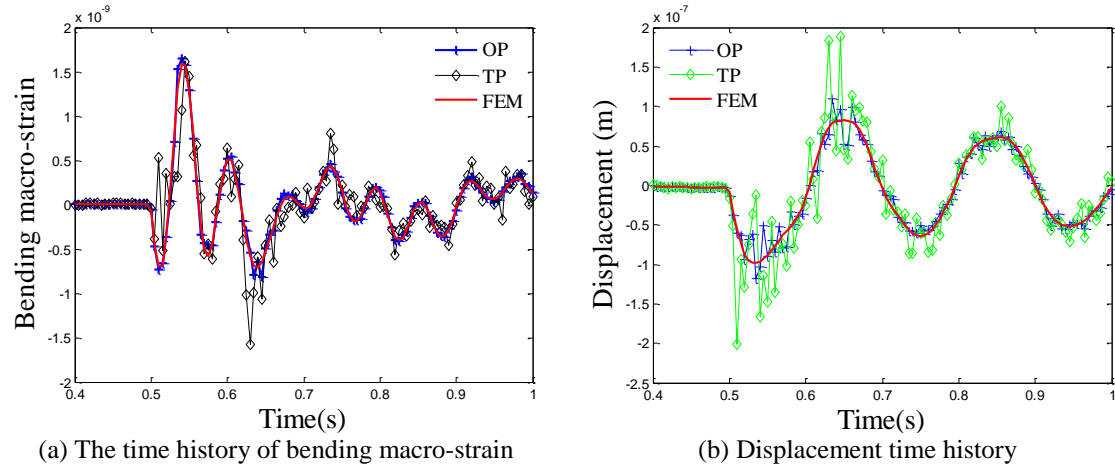
(a) The time history of bending macro-strain

(b) Displacement time history

Fig. 11 The time history curves from TP, OP and FEM

(a) 1.142kN
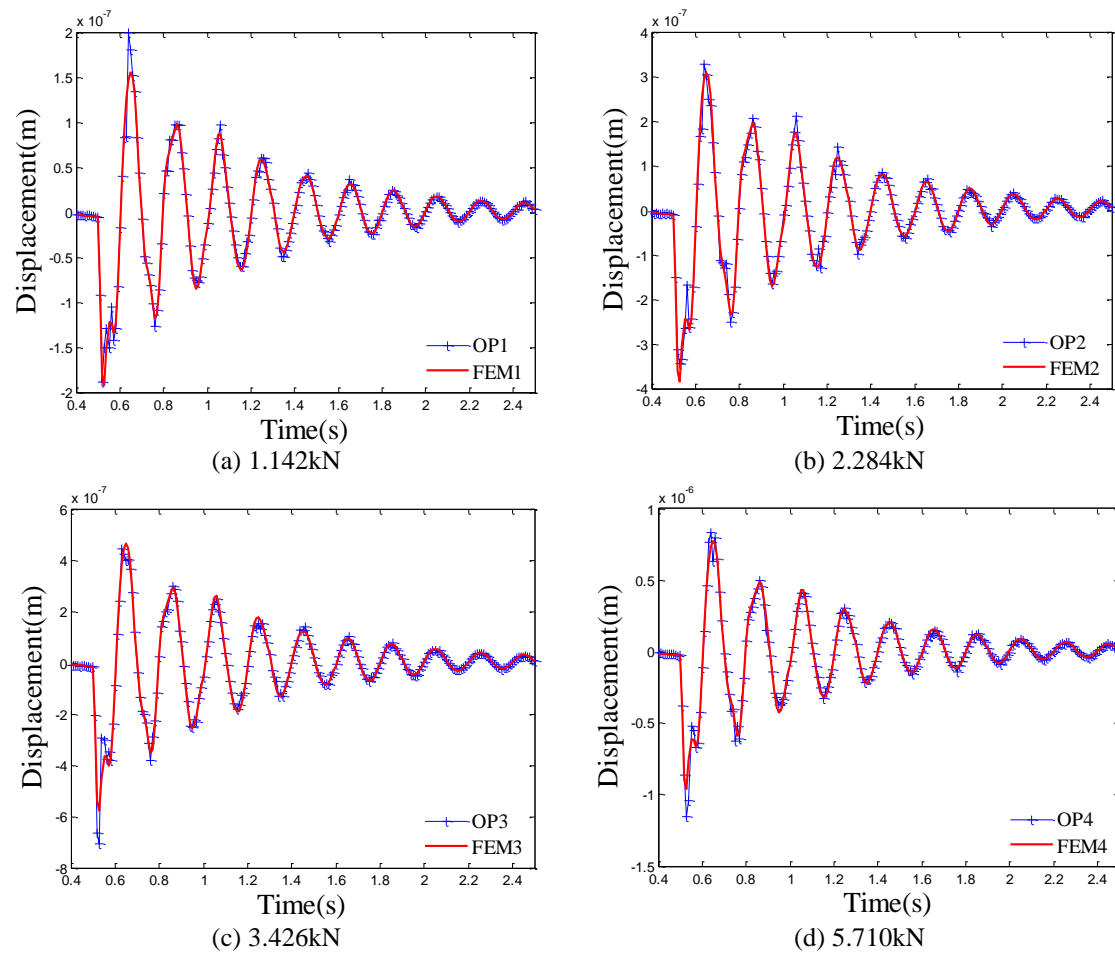
(b) 2.284kN

(c) 3.426kN

(d) 5.710kN

Fig.12 The time history of mid-span displacement under different impact force

The accuracy and robust of OP scheme is verified under different impact forces by analyzing and researching the time history of mid-span displacement. For the tied arch bridge, there are four impact forces that have been applied to the mid-span point whose amplitude is 1.142KN, 2.284KN, 3.426KN and 5.71KN respectively. The Fig. 12 shows the time histories of mid-span displacement under the four impact forces. It is seen that the mid-span displacement gradually rises with the increase of impact force from Fig. 12(a) to 12(d). The results indicate that the time histories of identified DD are basically same as the FEM under different impact forces.

According to the above-mentioned analysis, the proposed sensor layout framework is proved to be anti-noise and robust, which can be used for effectively identifying the deformation distribution.

5. Conclusions

An effective method of optimal sensor layout is proposed to identify the deformation distribution of tied arch bridge based on long-gauge fiber optic sensors in this article. For the optimal sensor layout framework, the most unfavorable load patterns and the general vehicle load state of the tied arch bridge are selected to be the target load conditions. Under these target load conditions, a characteristic curve of structure is firstly extracted by processing the bending macro-strain curves. In order to obtain the optimal sensor scheme, each group of the feature points in the characteristic curve with different number are chose by minimizing the error between the fitting curve and characteristic curve. Through the proposed optimal layout framework, multiple sensor layout schemes with different sensor number can be used for selection. For a structure, the proper sensor layout scheme can be applied for identifying the deformation distribution under static or dynamic load conditions. Compared with traditional sensor layout scheme, an example of tied arch bridge has been used to verify the proposed optimal sensor scheme. The identified results from the optimal sensor scheme are found to be in agreement with the finite element results, and the results can meet the requirement of precision. In addition, the results under multiple load conditions also show that the proposed optimal layout method has good anti-noise and robust performance.

Acknowledgements

References

Abdullah, M.M., Richardson, A. and Hanif, J. (2001), "Layout of sensors/actuators on civil structures using genetic algorithms", *Earthq. Eng. Struct. D.*, **30**, 1167-1184.
Buczak, A.L., Wang, H.H., Darabi, H. and Jafari, M.A. (2001), "Genetic algorithm convergence study for sensor network optimization", *Inform. Sci.*, **133**(3-4), 267-282.
He, X., She, T. and Zhao, L. (2012), "A new system for dynamic deflection measurement of highway bridge", *Appl. Mech. Mater.*, **226-228**, 1645-1650.
Heo, G., Wang, M. L., and Satpathi, D. (1997), "Optimal transducer layout for health monitoring of long

span bridge", *Soil. Dyn. Earthq. Eng*., **16**(7-8), 495-502.

Kammer, D.C. (1990), "Sensor layout for on-orbit modal identification and correlation of large space structures", *Proceedings of the American Control Conf.*, *IEEE*, New York.

Lei, Y. and Zheng, Z.P. (2013), "Review of physical based monitoring techniques for condition assessment of corrosion in reinforced concrete", *Math. Probl. Eng.*, Article ID 953930, 14 pages, http://dx.doi.org/10.1155/2013 /953930.

Meo, M. and Zumpano, G. (2005), "On the optimal sensor layout techniques for a bridge structure", *Eng. Struct.*, **27**(10), 1488-1497.

Papadopoulos, M. and Garcia, E. (1998), "Sensor layout methodologies for dynamic testing", *AIAA J.*, **36**(2), 256-263.

Shen, S., Wu, S.Z., Yang, C.Q., Wan, C.F., Tang, Y.S. and Wu, G. (2010), "An improved conjugated beam method for deformation monitoring with a distributed sensitive fiber optic sensor", *Struct. Health Monit.*, **9**(4), 361-378.

Worden, K. and Burrows, A.P. (2001), "Optimal sensor layout for fault detection", *Eng. Struct.*, **23**(8), 885-901.

Yau, M.H., Chan, T.H.T., Thambiratnam, D.P. and Tam, H.Y. (2013), "Static vertical displacement measurement of bridges using Fiber Bragg Grating (FBG) sensors", *Adv. Struct. Eng.*, **16**(1), 165-176.

Yi, T.H., Li, H.N. and Wang X. (2013), "Multi-dimensional sensor layout optimization for Canton Tower focusing on application demands", *Smart Struct. Syst.*, **12**(3-4), 235-250.

Yi, T.H., Li, H.N. and Zhang, X.D. (2015), "Health monitoring sensor layout optimization for Canton Tower using immune monkey algorithm", *Struct. Control Health*, **22**(1), 123-138.

Yung, B.L., Chang, K.C., Chern, J.C. and Wang, L.A. (2004), "The health monitoring of a prestressed concrete beam by using fiber Bragg grating sensors", *Smart Mater. Struct.*, **13**(4), 712-718.

Zhang, J., Hong, W., Tang, Y.S., Yang, C.Q., Wu, G. and Wu, Z.S. (2013), "Structural health monitoring of a steel stringer bridge with area sensing", *Structural and Infrastructural Engineering: Maintenance, Management, Life-Cycle Design and Performance*, DOI: 10.1080/15732479.2013.787103

Zhang, Q.Q., Zhang, J. and Wu, Z.S. (2015), "Deflection identification of the tied arch bridge from long-gauge strain", *Proceedings of the 7th International Society for Structural Health Monitoring of Intelligent Infrastructure*, July 1-3,Torino, Italy.

Zheng, Z., Lei, Y. and Sun, X. (2010), "Measuring corrosion of steels in concrete via fiber Bragg grating sensors—lab experimental test and in-field application", *Proceedings of the Earth and Space Conference*, Honolulu, Hawaii, USA.